Draft version October 20, 2025
Typeset using LaTeX **twocolumn** style in AASTeX631

Precise frequencies of $H_2{}^{16}O$ lines protected for radio astronomy

Arthémise Altman,[1] Roland Tóbiás,[2] Alexandr S. Bogomolov,[1] Meissa L. Diouf,[3] Frank M. J. Cozijn,[3] Attila G. Császár,[4] Clément Lauzin,[1] and Wim Ubachs[3]

[1] *Institute of Condensed Matter and Nanosciences, Université catholique de Louvain, Louvain-la-Neuve, Belgium*
[2] *Department of Chemistry, University of Vermont, Burlington, VT, 05405, USA &*
Institute of Chemistry, ELTE Eötvös Loránd University, H-1117 Budapest, Pázmány Péter sétány 1/A, Hungary
[3] *Department of Physics and Astronomy, LaserLaB, Vrije Universiteit, De Boelelaan 1100, 1081 HZ Amsterdam, The Netherlands*
[4] *Institute of Chemistry, ELTE Eötvös Loránd University, H-1518 Budapest, P.O. Box 32, Hungary*

ABSTRACT

Precise frequency values have been determined for $H_2{}^{16}O$ radio lines appearing in protected line lists of the International Astronomical Union and the Panel on Frequency Allocations of the US National Academy of Sciences. The improved precision is attributable to a spectroscopic network built from a large set of near-infrared Lamb-dip lines augmented with a handful of ultrahigh-accuracy rotational transitions. The ultraprecise $H_2{}^{16}O$ network contains 376 Lamb-dip lines recorded previously *via* our frequency-comb locked cavity-enhanced spectrometer. During the present study, altogether 55 target lines have been (re)measured at high accuracy. Due to our network-assisted measurements, the accuracy has been significantly improved with respect to previous direct radio-frequency measurements for all the protected lines of $H_2{}^{16}O$ between 750 and 3000 GHz. Furthermore, 43 of these protected transitions now benefit from the accuracy of the new near-infrared Lamb dips reported in this paper.

1. INTRODUCTION

The water molecule, H_2O, is one of the key species throughout the universe. It is made up of hydrogen, the most abundant element produced primordially, and oxygen, the third most abundant element produced in supernovae (van Dishoeck et al. 2013). Water molecules are synthesized in either gas-phase interactions (Solomon & Klemperer 1972) or *via* solid-state processes (Tielens & Hagen 1982) in interstellar space.

Water in the interstellar medium was discovered in the early days of radio astronomy (Cheung et al. 1969) through a 22 GHz maser line. Since then, the presence of water has been investigated *via* radio astronomical observations of the interstellar medium under various conditions (Wright et al. 2000; Cernicharo et al. 2006), using maser transitions as well as thermal spectral lines. In pushing the limits of radio astronomy, water was observed at a redshift of $z = 5.6$ (WeiĂź et al. 2013).

Datasets for reference frequencies of many molecular transitions, including those of $H_2{}^{16}O$, are maintained in numerous databases. In terms of radio astronomy, the most relevant databanks appear to be the Cologne Database for Molecular Spectroscopy (CDMS)[1] (Müller et al. 2005; Endres et al. 2016) and the Jet Propulsion Laboratory (JPL) line catalog[2] (Pickett et al. 1998).

At the XXIst General Assembly of the International Astronomical Union (IAU), taking place in Buenos Aires (July 23 – August 1, 1991), the astronomically most important spectral lines have been carefully reviewed. The need to protect the frequencies of these lines with some minimally line-specific band widths was defined. The original list covered 73 lines, of which four pertain to $H_2{}^{16}O$. Later, in preparation for the World Radiocommunication Conference 2000, held in Istanbul (May 8 – June 2, 2000), the IUCAF (Scientific Committee on Frequency Allocations for Radio Astronomy and Space Science) mm-wavelengths Working Group examined all known transitions in this region and specified revised allocations above 71 GHz. This catalog supplements the earlier list constructed by the IAU, extends to 1 THz, and covers in total 13 lines for $H_2{}^{16}O$. Both collections

Corresponding author: Wim Ubachs & Roland Tóbiás
w.m.g.ubachs@vu.nl & roland.tobias@ttk.elte.hu

[1] https://cdms.astro.uni-koeln.de/
[2] https://spec.jpl.nasa.gov/

can be accessed digitally.[3] Fifteen years later, the Panel on Frequency Allocations and Spectrum Protection for Scientific Uses of the US National Academy of Sciences (Committee on Radio Frequencies Board on Physics and Astronomy, National Academies of Sciences – Engineering – Medicine 2015) extended the list of protected water lines, in particular covering the frequency window between 1 and 3 THz, with 47 lines for $H_2{}^{16}O$ (here referred to as the NAS list). This leads to altogether 60 protected lines for the main isotopologue of water.

The principal aim of this investigation has been to provide frequency estimates with improved accuracy for the overwhelming majority of these 60 lines. To achieve this goal, laser-based precision-spectroscopy measurements were conducted for dozens of carefully chosen near-infrared transitions in the 1.2 – 1.4 μm range. Based on all the new and old kHz-accuracy transitions available for $H_2{}^{16}O$, an ultraprecise spectroscopic network (Császár & Furtenbacher 2011) was assembled, delivering highly accurate energies for 79 pure rotational states.

As shown in Ubachs et al. (2024), such ultraprecise spectroscopic networks facilitate the extraction of highly accurate frequencies for radio lines. In that study, the existing ultraprecise $H_2{}^{16}O$ and $H_2{}^{18}O$ networks were extended with newly measured Lamb-dip lines, enabling the derivation of accurate frequencies for a list of $H_2{}^{16}O$ maser transitions, as well as $H_2{}^{18}O$ lines observed extragalactically. Following this approach, the present work provides significantly refined frequency predictions for the protected $H_2{}^{16}O$ transitions, enhancing their reliability for future astronomical applications. The precise frequencies may find application in the accurate determination of velocities in astrophysical environments (Cazzoli et al. 2004).

2. ULTRAPRECISE $H_2{}^{16}O$ NETWORK

As to the notation used for the rovibrational states of $H_2{}^{16}O$, the vibrations are labelled with a triplet of normal-mode quantum numbers, $(v_1\, v_2\, v_3)$, where v_1, v_2, and v_3 represent the symmetric stretch, bend, and antisymmetric stretch motions, respectively. For the rotations, the rigid-rotor asymmetric-top quantum numbers J, K_a, and K_c are employed, in the form J_{K_a,K_c}. The rovibrational assignment of a transition is given here as $(v_1'\, v_2'\, v_3')J'_{K_a',K_c'} \leftarrow (v_1''\, v_2''\, v_3'')J''_{K_a'',K_c''}$, where $'$ and $''$ stand for its upper and lower states, respectively. Throughout the whole paper, only standard (NIST/SEMATECH 2012) uncertainties will be used.

In this study, the spectroscopic-network-assisted precision spectroscopy (SNAPS) procedure (Tóbiás et al. 2020) was applied to determine a large number of accurate transition frequencies, involving newly measured near-infrared Lamb-dip lines to form energy differences. These Lamb dips were recorded *via* laser-based Doppler-free saturation spectroscopy, yielding frequency uncertainties down to the kHz level. The superior sensitivity of the noise-immune cavity-enhanced optical-heterodyne molecular spectroscopy (NICE-OHMS) method (Gianfrani et al. 2024) is well-suited to detect weak lines, whose lower states have small population densities at room temperature. When combined with frequency-comb calibration, NICE-OHMS is suitable for providing absolute accuracy for the measured line positions.

In our previous experimental campaigns (Tóbiás et al. 2020; Diouf et al. 2022b; Tóbiás et al. 2024; Ubachs et al. 2024), several hundred $H_2{}^{16}O$ Lamb dips were measured, involving rovibrational states within polyads $P = 0$, 1, 4, and 5, where $P = 2v_1 + v_2 + 2v_3$ is the polyad number. Note, in particular, that ultrahigh-accuracy energies could be deduced for so-called hubs (that is, quantum states holding the largest number of transitions) in the full experimental $H_2{}^{16}O$ network (Furtenbacher et al. 2020a,b) available at that time (Tóbiás et al. 2024).

From the perspective of rovibrational spectroscopy, the quantum states of the $H_2{}^{16}O$ species, containing two equivalent hydrogen atoms with nuclear spin of $I = 1/2$, fall into four subnetworks. The *para*-$H_2{}^{16}O$ levels, with a total nuclear spin of $I = 0$, are fully separated from the *ortho*-$H_2{}^{16}O$ states, with $I = 1$, and no transitions between the states of these nuclear-spin isomers have ever been detected (Miani & Tennyson 2004). The *para*- and *ortho*-$H_2{}^{16}O$ levels are defined by $(-1)^{v_3+K_a+K_c}$ being $+1$ or -1, respectively. Within the (0 0 0) vibrational state, levels of opposite (total) parity cannot be linked *via* near-infrared dipole lines (note that *even*/*odd*-parity states have even/odd K_c values). Thus, when building a network from them, the even- and odd-parity subnetworks must be connected by pure rotational transitions.

One of the key features of spectroscopic networks is that their transitions form so-called paths and cycles (*i.e.*, series of connected lines, where the starting and ending states are different and identical, respectively). Paths are highly useful as they define energy differences between their starting and ending states, along with con-

[3] www.craf.eu/iau-list-of-important-spectral-lines/

servative uncertainty estimates. Cycles help not only to confirm the internal accuracy of the measurements, but also to check the self-consistency of the assignments. For further details, see Sec. 4 of Ubachs et al. (2024).

In the ultraprecise network built for $H_2{}^{16}O$, several microwave (Kukolich 1969; Golubiatnikov et al. 2006; Cazzoli et al. 2009) and near-infrared (Kassi et al. 2018; Chen et al. 2018; Tóbiás et al. 2020; Kassi et al. 2022; Diouf et al. 2022b; Tóbiás et al. 2024; Ubachs et al. 2024) transitions have been included. Following its latest update (Ubachs et al. 2024), this network now contains 411 previously measured microwave and near-infrared lines, where all the *ortho* (*para*) transitions form a single *ortho* (*para*) component.

3. NICE-OHMS MEASUREMENT CAMPAIGNS

To deduce kHz-accuracy frequencies for the protected $H_2{}^{16}O$ lines, a well-selected set of near-infrared lines was recorded *via* our NICE-OHMS setup at room temperature. The first part of the experiments was performed at LaserLaB Amsterdam, with the NICE-OHMS spectrometer developed there (Cozijn et al. 2018; Tóbiás et al. 2020). This setup was later moved to Louvain-la-Neuve, where the UCLouvain laboratory served as the site for the second set of measurements.

In the Amsterdam campaign, statistical averaging was carried out over four recordings per line. The frequency metrology was based on beat-note measurements against

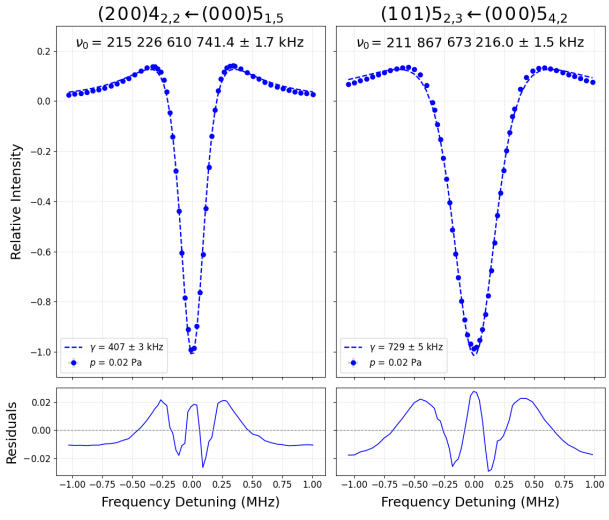

Figure 1. Examples for rovibrational Lamb-dip spectra measured for $H_2{}^{16}O$ *via* our NICE-OHMS setup. The γ parameters represent the full width at half maximum (FWHM) of the fitted Lorentzians. The frequency detuning is relative to the observed frequency, ν_0 (see also Table I).

a frequency-comb laser (Menlo Systems, FC1500), stabilized to a Cs clock (Microsemi CSIII), and long-term disciplined with respect to GPS. This yielded a frequency scale with negligible uncertainties compared to the statistical errors. The pressure-shift uncertainties were estimated using a worst-case pressure slope, found to be ± 20 kHz Pa^{-1} in our previous SNAPS studies (Tóbiás et al. 2020; Diouf et al. 2022b). Since the measurements were carried out at 0.01–0.02 Pa, this led to a pressure-induced uncertainty of 0.2–0.4 kHz. In the final uncertainties, the power-shift and day-to-day errors (0.5 and 1.5 kHz, respectively) were also taken into account.

For the measurement campaign at Louvain-la-Neuve, an automated scanning procedure was implemented, ensuring multiple recordings under stabilized conditions. All these experiments were conducted at 0.02 Pa, averaging over at least 16 scans, which gave rise to deviations typically below 1 kHz. At Louvain-la-Neuve, the frequency-comb laser (Toptica DFC Core+) was locked to a quartz oscillator clock, whose uncertainty was studied in a separate measurement campaign. This contribution is 0.9 kHz for the majority of lines averaged over 16 recordings, a somewhat larger value for averages over 8 scans, while for the four lines involved in long-term averaging over 100 scans this clock-related uncertainty becomes negligible. In the total uncertainty budget, the pressure-shift uncertainty, translating to 0.4 kHz at 0.02 Pa, was added as a linear term to the combined statistical (clock plus scan) uncertainty.

Figure 1 shows spectra of two new Lamb dips recorded at Louvain-la-Neuve and fitted using a derivative dispersion function (this model is well suited to wavelength-modulated NICE-OHMS signals). On the bottom panels of Fig. 1, the fitting residuals are also plotted, whose oscillating features are ascribed to effects due to the combination of high-frequency modulation with low frequency wavelength modulation, a phenomenon investigated in detail by Supplee et al. (1994). These oscillating features are characteristic of using a large modulation depth, where the signal deviates from a pure first-derivative line shape and contains contributions from higher-order derivatives of the dispersion profile. While this complicates a fully analytical description, the symmetry of these contributions ensures that their effect on the determination of the line center frequency is negligible. Note that the verification cycles, presented in Table S3, also demonstrate that the new lines are consistent within the claimed uncertainties.

Table I: New near-infrared Lamb-dip lines measured *via* an ultrasensitive NICE-OHMS spectrometer for $H_2{}^{16}O$.

NICE-OHMS (this work)[a]		Rovibrational assignment[b]	Previous results[c]/kHz		
Line frequency / kHz	p / Pa		Dev.	Unc.	Reference
209 966 584 532.4 ± 1.4	0.02	$(1\,0\,1)3_{1,3} \leftarrow (0\,0\,0)4_{3,2}$	–300	3000	Mikhailenko et al. (2018)
210 038 636 486.7 ± 1.4	0.02	$(2\,0\,0)5_{0,5} \leftarrow (0\,0\,0)5_{3,2}$	–3.7	10.4	Tóbiás et al. (2024)
210 463 484 645.5 ± 1.5	0.02	$(0\,2\,1)6_{3,4} \leftarrow (0\,0\,0)6_{1,5}$	500	3000	Mikhailenko et al. (2018)
210 664 080 420.2 ± 1.3	0.02	$(0\,2\,1)6_{5,1} \leftarrow (0\,0\,0)7_{3,4}$	–21 800	3000	Mikhailenko et al. (2018)
211 120 145 834.0 ± 1.5	0.02	$(2\,0\,0)5_{4,2} \leftarrow (0\,0\,0)5_{5,1}$	–5.2	3.0	Ubachs et al. (2024)
211 126 350 475.9 ± 1.5	0.02	$(2\,0\,0)5_{4,1} \leftarrow (0\,0\,0)5_{5,0}$	–0.3	11.1	Tóbiás et al. (2024)
211 545 072 422.8 ± 1.5	0.02	$(1\,0\,1)2_{1,1} \leftarrow (0\,0\,0)3_{3,0}$	–0.8	7.5	Tóbiás et al. (2024)
211 630 806 780.1 ± 0.6	0.02	$(0\,2\,1)6_{3,4} \leftarrow (0\,0\,0)5_{3,3}$	100	3000	Mikhailenko et al. (2018)
211 802 311 374.9 ± 1.4	0.02	$(2\,0\,0)6_{3,4} \leftarrow (0\,0\,0)6_{4,3}$	–9.6	10.0	Tóbiás et al. (2024)
211 867 673 216.0 ± 1.5	0.02	$(1\,0\,1)5_{2,3} \leftarrow (0\,0\,0)5_{4,2}$	–0.2	7.7	Tóbiás et al. (2024)
212 286 960 311.8 ± 1.4	0.02	$(2\,0\,0)6_{3,3} \leftarrow (0\,0\,0)6_{4,2}$	2.5	10.4	Tóbiás et al. (2024)
212 549 726 956.5 ± 1.5	0.02	$(2\,0\,0)4_{2,3} \leftarrow (0\,0\,0)5_{1,4}$	1.3	7.5	Diouf et al. (2022b)
212 843 780 340.2 ± 1.4	0.02	$(2\,0\,0)5_{1,5} \leftarrow (0\,0\,0)5_{2,4}$	3.2	7.6	Diouf et al. (2022b)
212 877 518 672.9 ± 1.8	0.02	$(1\,0\,1)3_{1,3} \leftarrow (0\,0\,0)3_{3,0}$	300	3000	Mikhailenko et al. (2018)
213 248 005 986.5 ± 1.7	0.02	$(2\,0\,0)3_{2,2} \leftarrow (0\,0\,0)3_{3,1}$	1.5	5.2	Tóbiás et al. (2020)
213 317 003 150.6 ± 1.8	0.02	$(2\,0\,0)5_{0,5} \leftarrow (0\,0\,0)5_{1,4}$	1.2	7.6	Diouf et al. (2022b)
213 376 695 569.3 ± 1.3	0.02	$(2\,0\,0)4_{1,4} \leftarrow (0\,0\,0)4_{2,3}$	–7.3	8.2	Tóbiás et al. (2024)
213 394 923 797.3 ± 1.4	0.02	$(2\,0\,0)6_{5,2} \leftarrow (0\,0\,0)7_{4,3}$	5.2	2.4	Tóbiás et al. (2020)
213 446 816 436.0 ± 1.6	0.02	$(2\,0\,0)3_{2,1} \leftarrow (0\,0\,0)3_{3,0}$	2.5	2.4	Tóbiás et al. (2020)
213 511 286 802.5 ± 1.4	0.02	$(2\,0\,0)4_{2,2} \leftarrow (0\,0\,0)4_{3,1}$	4.8	12.1	Tóbiás et al. (2024)
213 526 600 994.6 ± 1.6	0.02	$(2\,0\,0)6_{2,4} \leftarrow (0\,0\,0)6_{3,3}$	0.4	5.1	Tóbiás et al. (2024)
213 534 197 981.2 ± 1.5	0.02	$(2\,0\,0)5_{4,2} \leftarrow (0\,0\,0)6_{3,3}$	1.6	7.5	Diouf et al. (2022b)
213 539 473 234.3 ± 1.5	0.02	$(2\,0\,0)3_{2,2} \leftarrow (0\,0\,0)4_{1,3}$	–1.1	5.1	Tóbiás et al. (2024)
213 663 124 477.7 ± 2.0	0.01	$(2\,0\,0)2_{0,2} \leftarrow (0\,0\,0)3_{1,3}$	2.8	7.6	Tóbiás et al. (2024)
213 670 408 312.7 ± 1.4	0.02	$(0\,2\,1)6_{5,1} \leftarrow (0\,0\,0)5_{5,0}$	–1300	3000	Mikhailenko et al. (2018)
213 731 119 700.4 ± 0.7	0.02	$(2\,0\,0)6_{3,3} \leftarrow (0\,0\,0)7_{2,6}$	–14.6	11.9	Tóbiás et al. (2024)
213 810 471 367.1 ± 1.9	0.02	$(2\,0\,0)3_{1,3} \leftarrow (0\,0\,0)3_{2,2}$	0.9	5.3	Tóbiás et al. (2020)
213 917 346 155.5 ± 1.8	0.02	$(2\,0\,0)5_{4,1} \leftarrow (0\,0\,0)6_{3,4}$	0.3	7.5	Diouf et al. (2022b)
214 699 466 014.1 ± 1.8	0.01	$(2\,0\,0)4_{4,0} \leftarrow (0\,0\,0)5_{3,3}$	1.5	3.2	Tóbiás et al. (2024)
215 226 610 741.4 ± 1.7	0.02	$(2\,0\,0)4_{2,2} \leftarrow (0\,0\,0)5_{1,5}$	8.7	10.4	Tóbiás et al. (2024)
215 262 964 876.7 ± 1.7	0.02	$(2\,0\,0)3_{2,1} \leftarrow (0\,0\,0)4_{1,4}$	6.7	8.0	Tóbiás et al. (2024)
215 412 696 377.0 ± 1.2	0.02	$(2\,0\,0)5_{2,3} \leftarrow (0\,0\,0)6_{1,6}$	0.5	7.5	Diouf et al. (2022b)
215 524 549 225.1 ± 1.7	0.02	$(1\,0\,1)5_{2,3} \leftarrow (0\,0\,0)4_{4,0}$	2.6	2.6	Tóbiás et al. (2020)
215 531 118 312.8 ± 1.9	0.01	$(2\,0\,0)2_{2,0} \leftarrow (0\,0\,0)3_{1,3}$	3.7	2.4	Tóbiás et al. (2020)
215 854 572 219.6 ± 2.1	0.02	$(2\,0\,0)5_{1,5} \leftarrow (0\,0\,0)4_{2,2}$	4.4	7.7	Diouf et al. (2022b)
215 968 528 397.7 ± 1.7	0.02	$(2\,0\,0)4_{2,3} \leftarrow (0\,0\,0)3_{3,0}$	12.4	4.9	Tóbiás et al. (2024)
216 021 042 445.5 ± 1.6	0.02	$(2\,0\,0)4_{1,4} \leftarrow (0\,0\,0)3_{2,1}$	–7.6	4.9	Tóbiás et al. (2024)
216 269 473 019.8 ± 1.4	0.02	$(1\,0\,1)4_{3,1} \leftarrow (0\,0\,0)5_{1,4}$	0.5	5.3	Tóbiás et al. (2020)
216 320 509 854.1 ± 1.3	0.02	$(0\,0\,2)4_{1,4} \leftarrow (0\,0\,0)5_{2,3}$	500	3000	Mikhailenko et al. (2018)
216 467 935 089.8 ± 1.9	0.02	$(2\,0\,0)4_{2,2} \leftarrow (0\,0\,0)3_{3,1}$	7.2	4.9	Tóbiás et al. (2024)
216 766 816 926.4 ± 1.9	0.02	$(1\,0\,1)5_{2,3} \leftarrow (0\,0\,0)6_{0,6}$	4.5	2.4	Tóbiás et al. (2020)
216 815 183 206.7 ± 4.6	0.01	$(2\,0\,0)2_{0,2} \leftarrow (0\,0\,0)1_{1,1}$	–0.8	9.5	Tóbiás et al. (2024)
216 913 210 411.2 ± 1.7	0.02	$(2\,0\,0)6_{3,4} \leftarrow (0\,0\,0)7_{0,7}$	–3.1	3.1	Tóbiás et al. (2024)
216 943 217 125.0 ± 1.8	0.01	$(2\,0\,0)2_{2,0} \leftarrow (0\,0\,0)2_{1,1}$	2.9	5.6	Tóbiás et al. (2020)
217 353 416 776.9 ± 1.4	0.02	$(2\,0\,0)5_{2,3} \leftarrow (0\,0\,0)4_{3,2}$	16.5	11.4	Tóbiás et al. (2024)
217 533 265 067.6 ± 1.5	0.02	$(2\,0\,0)3_{2,2} \leftarrow (0\,0\,0)3_{1,3}$	3.4	5.5	Tóbiás et al. (2020)
217 680 819 618.1 ± 1.7	0.01	$(1\,0\,1)5_{2,3} \leftarrow (0\,0\,0)5_{2,4}$	3.0	6.5	Tóbiás et al. (2024)
217 893 962 755.6 ± 1.5	0.02	$(2\,0\,0)3_{1,3} \leftarrow (0\,0\,0)2_{0,2}$	–0.8	5.2	Tóbiás et al. (2020)
218 089 528 336.1 ± 1.4	0.02	$(2\,0\,0)5_{2,4} \leftarrow (0\,0\,0)5_{1,5}$	8.6	7.9	Tóbiás et al. (2024)
218 300 740 560.6 ± 1.5	0.02	$(2\,0\,0)4_{4,0} \leftarrow (0\,0\,0)4_{3,1}$	1.5	5.2	Tóbiás et al. (2020)

Continued on next page

Table I – *Continued from previous page*

NICE-OHMS (this work)[a]		Rovibrational assignment[b]	Previous results[c]		
Line frequency / kHz	p / Pa		Dev.	Unc.	Reference
218 430 303 226.9 ± 0.6	0.02	$(2\,0\,0)6_{2,5} \leftarrow (0\,0\,0)6_{1,6}$	3.2	7.5	Diouf et al. (2022b)
218 683 177 038.4 ± 1.4	0.02	$(2\,0\,0)2_{2,0} \leftarrow (0\,0\,0)1_{1,1}$	3.5	5.2	Tóbiás et al. (2020)
219 622 319 932.4 ± 1.4	0.02	$(2\,0\,0)5_{2,4} \leftarrow (0\,0\,0)4_{1,3}$	2.4	7.6	Diouf et al. (2022b)
219 863 156 322.3 ± 0.7	0.02	$(2\,0\,0)6_{2,5} \leftarrow (0\,0\,0)5_{1,4}$	7.3	11.2	Tóbiás et al. (2024)
219 952 878 188.5 ± 1.4	0.02	$(0\,0\,2)4_{1,4} \leftarrow (0\,0\,0)5_{0,5}$	900	3000	Mikhailenko et al. (2018)

[a] New Lamb-dip frequencies, with their standard (NIST/SEMATECH 2012) uncertainties, at pressures displayed in column "p". The nine italicized frequencies were recorded at Amsterdam in 2024, while the other positions were measured at Louvain-la-Neuve in 2025.
[b] The rovibrational assignments are given as $(v_1'\,v_2'\,v_3')J'_{K_a',K_c'} \leftarrow (v_1''\,v_2''\,v_3'')J''_{K_a'',K_c''}$ (see also Sec. 2).
[c] Best literature results, corresponding to previous (Lamb-dip and Doppler-limited) experimental line positions or taken from a SNAPS analysis performed in Tóbiás et al. (2024). The column "Dev." lists the deviations of the previous frequency values from those reported in the first column. The column "Unc." contains standard uncertainties provided in the cited publications. The deviations, apart from the two underlined cases, remain within the claimed expanded (two-sigma) uncertainties (NIST/SEMATECH 2012).

Table II: Improved frequencies for protected $H_2{}^{16}O$ lines provided in the IAU/CRAF and NAS lists.

Line frequency		Rovibrational assignment[b]	24SNAPS[d,e] / kHz		Best measured[c,e] / kHz		
Rest[a] / GHz	Recommended[b,e] / kHz		Dev.	Unc.	Dev.	Unc.	Reference
22.235	*22 235 079.85 ± 0.05*	$(0\,0\,0)6_{1,6} \leftarrow (0\,0\,0)5_{2,3}$	0	0.05	0	0.05	Kukolich (1969)
183.310	*183 310 087.0 ± 1.0*	$(0\,0\,0)3_{1,3} \leftarrow (0\,0\,0)2_{2,0}$	0	1.0	0	1	Golubiatnikov et al. (2006)
325.153	*325 152 899.0 ± 1.0*	$(0\,0\,0)5_{1,5} \leftarrow (0\,0\,0)4_{2,2}$	0	1.0	0	1	Golubiatnikov et al. (2006)
380.197	*380 197 359.8 ± 0.1*	$(0\,0\,0)4_{1,4} \leftarrow (0\,0\,0)3_{2,1}$	0	0.1	0	0.1	Cazzoli et al. (2009)
439.151	*439 150 794.8 ± 0.3*	$(0\,0\,0)6_{4,3} \leftarrow (0\,0\,0)5_{5,0}$	0	0.3	0	0.3	Cazzoli et al. (2009)
448.001	*448 001 077.5 ± 0.5*	$(0\,0\,0)4_{2,3} \leftarrow (0\,0\,0)3_{3,0}$	0	0.5	0	0.5	Cazzoli et al. (2009)
474.689	*474 689 108.0 ± 1.0*	$(0\,0\,0)5_{3,3} \leftarrow (0\,0\,0)4_{4,0}$	0	1.0	0	1	Golubiatnikov et al. (2006)
556.936	*556 935 987.7 ± 0.3*	$(0\,0\,0)1_{1,0} \leftarrow (0\,0\,0)1_{0,1}$	0	0.3	0	0.3	Cazzoli et al. (2009)
620.700	*620 700 954.9 ± 0.6*	$(0\,0\,0)5_{3,2} \leftarrow (0\,0\,0)4_{4,1}$	0	0.6	0	0.6	Cazzoli et al. (2009)
752.033	752 033 122.7 ± 3.5	$(0\,0\,0)2_{1,1} \leftarrow (0\,0\,0)2_{0,2}$	0	8.2	–19	13	Matsushima et al. (1995)
916.172	916 171 449.4 ± 2.7	$(0\,0\,0)4_{2,2} \leftarrow (0\,0\,0)3_{3,1}$	0.5	8.3	–44	13	Matsushima et al. (1995)
970.315	970 315 041.5 ± 3.5	$(0\,0\,0)5_{2,4} \leftarrow (0\,0\,0)4_{3,1}$	3.6	9.4	–73	18	Matsushima et al. (1995)
987.927	987 926 790.7 ± 3.3	$(0\,0\,0)2_{0,2} \leftarrow (0\,0\,0)1_{1,1}$	0.6	7.9	–48	16	Matsushima et al. (1995)
1 097.365	1 097 364 863.4 ± 5.4	$(0\,0\,0)3_{1,2} \leftarrow (0\,0\,0)3_{0,3}$	–0.8	6.4	–72	13	Matsushima et al. (1995)
1 113.343	1 113 343 013.8 ± 4.8	$(0\,0\,0)1_{1,1} \leftarrow (0\,0\,0)0_{0,0}$	0.2	7.1	–50	16	Matsushima et al. (1995)
1 153.127	1 153 126 821.0 ± 4.4	$(0\,0\,0)3_{1,2} \leftarrow (0\,0\,0)2_{2,1}$	–0.8	6.3	1	13	Matsushima et al. (1995)
1 158.324	1 158 323 846.3 ± 7.3	$(0\,0\,0)6_{3,4} \leftarrow (0\,0\,0)5_{4,1}$	0	7.3	–103	25	Matsushima et al. (1995)
1 162.912	1 162 911 605.0 ± 2.6	$(0\,0\,0)3_{2,1} \leftarrow (0\,0\,0)3_{1,2}$	1.1	8.7	–12	13	Matsushima et al. (1995)
1 207.639	1 207 638 697.3 ± 2.2	$(0\,0\,0)4_{2,2} \leftarrow (0\,0\,0)4_{1,3}$	–2.2	8.2	17	13	Matsushima et al. (1995)
1 228.789	1 228 788 725.2 ± 2.8	$(0\,0\,0)2_{2,0} \leftarrow (0\,0\,0)2_{1,1}$	–0.8	6.2	47	13	Matsushima et al. (1995)
1 322.065	1 322 064 738.5 ± 5.4	$(0\,0\,0)6_{2,5} \leftarrow (0\,0\,0)5_{3,2}$	0	5.4	65	13	Matsushima et al. (1995)
1 410.618	1 410 618 015.5 ± 0.9	$(0\,0\,0)5_{2,3} \leftarrow (0\,0\,0)5_{1,4}$	18.9	8.7	58	13	Matsushima et al. (1995)
1 440.782	1 440 781 661.6 ± 3.3	$(0\,0\,0)7_{2,6} \leftarrow (0\,0\,0)6_{3,3}$	23.4	9.0	7	20	Yu et al. (2012)
1 541.967	1 541 967 023.2 ± 3.3	$(0\,0\,0)6_{3,3} \leftarrow (0\,0\,0)5_{4,2}$	–3.2	9.7	–238	23	Matsushima et al. (1995)
1 602.219	1 602 219 231.7 ± 3.4	$(0\,0\,0)4_{1,3} \leftarrow (0\,0\,0)4_{0,4}$	4.5	8.0	–50	16	Matsushima et al. (1995)
1 661.008	1 661 007 733.5 ± 4.0	$(0\,0\,0)2_{2,1} \leftarrow (0\,0\,0)2_{1,2}$	0	4.0	–96	22	Matsushima et al. (1995)
1 669.905	1 669 904 804.7 ± 3.0	$(0\,0\,0)2_{1,2} \leftarrow (0\,0\,0)1_{0,1}$	0	3.0	–30	37	Matsushima et al. (1995)
1 713.883	1 713 883 014.3 ± 2.7	$(0\,0\,0)4_{3,2} \leftarrow (0\,0\,0)5_{0,5}$	–14.5	9.7	–41	13	Matsushima et al. (1995)
1 716.770	1 716 769 691.1 ± 4.2	$(0\,0\,0)3_{0,3} \leftarrow (0\,0\,0)2_{1,2}$	0	4.2	–58	13	Matsushima et al. (1995)
1 716.957	1 716 956 809.3 ± 2.7	$(0\,0\,0)5_{3,3} \leftarrow (0\,0\,0)6_{0,6}$	1.9	3.7	–20	50	Yu et al. (2013)

Continued on next page

Table II – *Continued from previous page*

Line frequency		Rovibrational assignment[b]	24SNAPS[d,e] / kHz		Best measured[c,e] / kHz		
Rest[a] / GHz	Recommended[b,e] / kHz		Dev.	Unc.	Dev.	Unc.	Reference
1 762.043	1 762 042 823.3 ± 4.6	$(0\,0\,0)6_{3,3} \leftarrow (0\,0\,0)6_{2,4}$	–0.4	6.7	–32	13	Matsushima et al. (1995)
1 794.789	1 794 788 968.0 ± 4.6	$(0\,0\,0)6_{2,4} \leftarrow (0\,0\,0)6_{1,5}$	0.7	6.8	–15	13	Matsushima et al. (1995)
1 867.749	1 867 748 648.3 ± 2.5	$(0\,0\,0)5_{3,2} \leftarrow (0\,0\,0)5_{2,3}$	–4.8	5.1	–54	13	Matsushima et al. (1995)
1 880.753	1 880 752 561.9 ± 3.2	$(0\,0\,0)6_{3,4} \leftarrow (0\,0\,0)7_{0,7}$	–4.3	8.7	39	50	Yu et al. (2012)
1 893.687	1 893 686 479.5 ± 3.5	$(0\,0\,0)3_{3,1} \leftarrow (0\,0\,0)4_{0,4}$	1.9	8.0	33	50	Yu et al. (2012)
1 918.485	1 918 485 320.0 ± 1.8	$(0\,0\,0)5_{2,3} \leftarrow (0\,0\,0)4_{3,2}$	16.0	8.6	4	16	Matsushima et al. (1995)
1 919.360	1 919 359 453.6 ± 2.6	$(0\,0\,0)3_{2,2} \leftarrow (0\,0\,0)3_{1,3}$	–0.9	5.6	77	13	Matsushima et al. (1995)
2 014.865	2 014 864 766.5 ± 3.0	$(0\,0\,0)5_{4,2} \leftarrow (0\,0\,0)6_{1,5}$	5.1	9.8	95	50	Yu et al. (2013)
2 040.477	2 040 476 837.9 ± 2.4	$(0\,0\,0)4_{3,1} \leftarrow (0\,0\,0)4_{2,2}$	3.9	6.3	–28	20	Matsushima et al. (1995)
2 074.432	2 074 432 379.7 ± 3.3	$(0\,0\,0)4_{1,3} \leftarrow (0\,0\,0)3_{2,2}$	5.4	9.3	–75	16	Matsushima et al. (1995)
2 164.132	2 164 131 934.9 ± 2.3	$(0\,0\,0)3_{1,3} \leftarrow (0\,0\,0)2_{0,2}$	–0.8	5.5	45	18	Matsushima et al. (1995)
2 196.346	2 196 345 798.7 ± 2.1	$(0\,0\,0)3_{3,0} \leftarrow (0\,0\,0)3_{2,1}$	–0.3	6.6	–43	16	Matsushima et al. (1995)
2 221.751	2 221 750 318.8 ± 2.1	$(0\,0\,0)5_{1,4} \leftarrow (0\,0\,0)5_{0,5}$	–17.4	9.7	181	18	Matsushima et al. (1995)
2 264.150	2 264 149 516.4 ± 2.1	$(0\,0\,0)4_{2,3} \leftarrow (0\,0\,0)4_{1,4}$	–0.3	6.6	134	13	Matsushima et al. (1995)
2 344.290	2 344 250 440.9 ± 6.6	$(0\,0\,0)7_{2,5} \leftarrow (0\,0\,0)7_{1,6}$	0	6.6	–106	18	Matsushima et al. (1995)
2 365.900	2 365 899 627.5 ± 3.4	$(0\,0\,0)3_{3,1} \leftarrow (0\,0\,0)3_{2,2}$	2.8	9.4	31	20	Matsushima et al. (1995)
2 391.573	2 391 572 601.6 ± 2.6	$(0\,0\,0)4_{0,4} \leftarrow (0\,0\,0)3_{1,3}$	0	2.6	26	13	Matsushima et al. (1995)
2 462.933	2 462 933 063.0 ± 2.3	$(0\,0\,0)4_{3,2} \leftarrow (0\,0\,0)4_{2,3}$	–4.2	7.5	–31	13	Matsushima et al. (1995)
2 630.960	2 630 959 501.0 ± 2.6	$(0\,0\,0)5_{3,3} \leftarrow (0\,0\,0)5_{2,4}$	0.4	7.1	19	27	Matsushima et al. (1995)
2 640.474	2 640 473 835.2 ± 5.6	$(0\,0\,0)4_{1,4} \leftarrow (0\,0\,0)3_{0,3}$	–6.7	6.8	–22	3	Drouin et al. (2011)
2 657.666	2 657 665 709.0 ± 2.4	$(0\,0\,0)4_{4,1} \leftarrow (0\,0\,0)5_{1,4}$	14.0	8.1	81	50	Chance et al. (1998)
2 664.561	2 664 570 686.1 ± 2.8	$(0\,0\,0)7_{4,3} \leftarrow (0\,0\,0)7_{3,4}$	–2.6	9.3	18	16	Matsushima et al. (1995)
2 685.639	2 685 638 980.4 ± 2.7	$(0\,0\,0)5_{2,4} \leftarrow (0\,0\,0)5_{1,5}$	7.1	7.8	–11	18	Matsushima et al. (1995)
2 773.977	2 773 976 550.5 ± 2.7	$(0\,0\,0)2_{2,1} \leftarrow (0\,0\,0)1_{1,0}$	0	2.7	38	20	Matsushima et al. (1995)
2 880.025	2 880 025 391.7 ± 3.9	$(0\,0\,0)6_{3,4} \leftarrow (0\,0\,0)6_{2,5}$	–1.1	7.6	–23	30	Matsushima et al. (1995)
2 884.279	2 884 278 943.9 ± 3.2	$(0\,0\,0)6_{1,5} \leftarrow (0\,0\,0)6_{0,6}$	–0.4	6.6	–4	18	Matsushima et al. (1995)
2 884.941	2 884 941 050.2 ± 2.9	$(0\,0\,0)6_{4,2} \leftarrow (0\,0\,0)6_{3,3}$	6.3	7.0	2	18	Matsushima et al. (1995)
2 962.111	2 962 111 102.6 ± 4.3	$(0\,0\,0)6_{2,4} \leftarrow (0\,0\,0)5_{3,3}$	–1.6	4.6	–9	16	Matsushima et al. (1995)
2 968.749	2 968 748 638.6 ± 2.6	$(0\,0\,0)2_{2,0} \leftarrow (0\,0\,0)1_{1,1}$	–0.2	5.8	15	16	Matsushima et al. (1995)
2 970.800	2 970 800 363.7 ± 2.3	$(0\,0\,0)5_{1,4} \leftarrow (0\,0\,0)4_{2,3}$	–3.3	7.6	–120	16	Matsushima et al. (1995)

[a] Approximate ("rest") frequencies extracted from the primary and supplementary IAU/CRAF reference lists (below 1 THz) or the NAS catalog (above 1 THz). The 2631.051 and 2970.801 GHz frequencies, which correspond to the same rovibrational transitions as the 2 630.960 and 2 970.800 GHz values, respectively, are not included in this table.
[b] Recommended transition frequencies ± standard (NIST/SEMATECH 2012) uncertainties, derived in the present work *via* the SNAPS scheme and attached with their rovibrational assignments. Most of these values rely on the new Lamb-dip frequencies given in Table I.
[c] The most accurate laboratory measurements taken from the literature. The 6th column ("Dev.") contains the deviations of the measured positions from the recommended frequencies. The 7th column ("Unc.") includes the standard uncertainties taken from the individual data sources. The experimental position of the 2 640.474 GHz line, reported in Drouin et al. (2011), does not reflect the zero pressure value, as it was recorded at a pressure higher than 100 Pa, without pressure correction.
[d] SNAPS estimates utilizing the previous version of the ultraprecise $H_2{}^{16}O$ network considered in Ubachs et al. (2024).
[e] The recommended frequencies typeset in italics fully coincide with their direct experimental counterparts, leading to zero deviations in the 6th ("Dev.") column. Similarly, where zero deviations are reported in the 4th ("Dev.") column, the recommended values do not benefit from the newly measured Lamb dips.

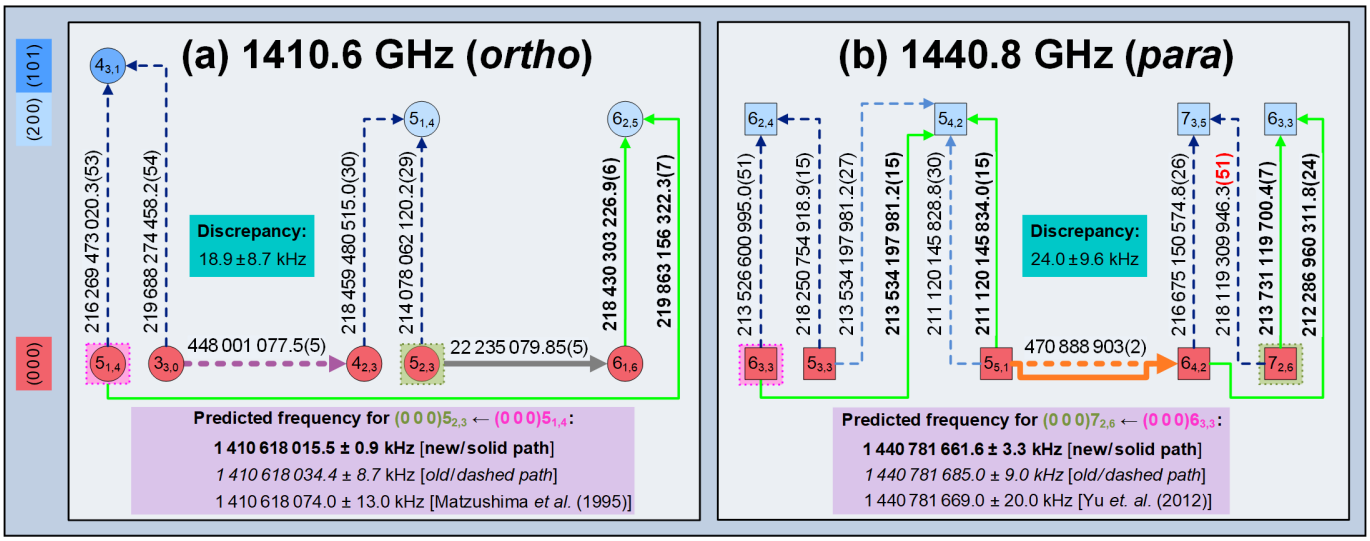

Figure 2. Comparison of new and previous kHz-accuracy paths for two selected radio lines of Table II. The *ortho* and *para* states of this figure are designated with circles and squares, respectively. For these energy levels, the J_{K_a,K_c} labels are written out explicitly, while the $(v_1\, v_2\, v_3)$ triplets are shown in the left-side color legend. The green arrows denote new Lamb-dip transitions, while those in dark blue, gray, orange, purple, and light blue are extremely accurate lines collected from Tóbiás et al. (2020), Kukolich (1969), Golubiatnikov et al. (2006), Cazzoli et al. (2009), and Ubachs et al. (2024), respectively. For the pure rotational transitions included on the paths, the arrows are thickened. The numbers on the arrows are frequencies in kHz, with the standard (NIST/SEMATECH 2012) uncertainties of the last digits in parentheses. The solid arrows constitute the new (smallest-uncertainty) paths between their starting and ending states, surrounded by dotted magenta and green boxes, respectively. The red uncertainty value was slightly underestimated in Tóbiás et al. (2020), the true uncertainty must be around 15 kHz. The dashed arrows represent the previous paths, forming cycles with the solid ones. The orange line, illustrated as a double arrow, is part of both paths. The rest frequencies, related to lines between the starting and ending states of the two paths, are placed at the top of both panels. The light mauve and teal blue boxes provide predicted frequencies and discrepancies, along with their standard uncertainties, respectively. The direct experimental values are also listed in the mauve boxes. These two examples correspond to the highest improvements achieved for the protected *ortho*- and *para*-$H_2{}^{16}O$ transitions.

The list of 55 lines, measured during this study for $H_2{}^{16}O$, is presented in Table I, where the nine frequencies recorded in Amsterdam are typeset in italics. The typical accuracy of the new measurements is around 2 kHz, thereby improving upon our previous experimental (Tóbiás et al. 2020; Diouf et al. 2022b) or SNAPS-predicted (Tóbiás et al. 2024) line-center positions. For eight transitions, only Doppler-broadened observations were previously available, with a claimed uncertainty of 3 MHz (Mikhailenko et al. 2018).

4. NETWORK-BASED FREQUENCY PREDICTIONS

The ultraprecise $H_2{}^{16}O$ network, augmented with the newly measured lines presented in Table I, was used to extract highly accurate frequencies for radio lines. Figure 2 illustrates how the predicted frequencies have been extended from this network, applying the Ritz principle (Ritz 1908) in a successive fashion.

In these examples, a connection has to be made between opposite-parity levels in the ground vibrational state and an odd number of known rotational lines must be included. The first nine IAU/CRAF transitions, see Table II, which were measured at an accuracy better than 1 kHz in microwave studies (Kukolich 1969; Golubiatnikov et al. 2006; Cazzoli et al. 2009), serve this purpose. This extreme precision could be achieved only for one SNAPS prediction, see Fig. 2(a), relying on two of the four sub-kHz accuracy lines reported in Table I.

For the remaining 51 lines in Table II, all part of the IAU/CRAF and NAS lists, the frequencies could be improved, on average, by a factor of 3, with respect to our previous SNAPS analysis (Tóbiás et al. 2024), and even better when compared to the direct terahertz measurements (Matsushima et al. 1995; Chance et al. 1998; Drouin et al. 2011; Yu et al. 2012). The new network-assisted measurements made it possible to utilize the sub-kHz accuracy near-infrared transition of Kassi et al. (2022), yielding a frequency uncertainty of 2.6 kHz for the 1163 GHz line. For a comparison of the various frequency estimates available for the protected $H_2{}^{16}O$

lines (Townes & Merritt 1946; Golden et al. 1948; Jen 1951; King & Gordy 1954; Kukolich 1969; Stephenson & Strauch 1970; Huiszoon 1971; Steenbeckeliers & Bellet 1971; Flaud et al. 1972; de Lucia et al. 1972; Fleming & Gibson 1976; Kauppinen et al. 1978; Kauppinen & Kyrö 1980; Partridge 1981; Burenin et al. 1983; Helminger et al. 1983; Messer et al. 1983; Johns 1985; Guelachvili & Rao 1986; Bauer et al. 1989; Markov & Krupnov 1995; Matsushima et al. 1995; Brown & Plymate 1996; Bauer et al. 1998; Chance et al. 1998; Coudert et al. 2004; Golubiatnikov 2005; Golubiatnikov et al. 2006; Koshelev et al. 2007; Cazzoli et al. 2009; Drouin et al. 2011; Koshelev 2011; Yu et al. 2012; Tretyakov et al. 2013; Yu et al. 2013; Coudert et al. 2014; Mikhailenko et al. 2020; Tóbiás et al. 2020; Diouf et al. 2022b; Toureille et al. 2022; Karlovets et al. 2024; Mikhailenko et al. 2024), see the Supplemental Information.

It should be stressed that all transition frequencies included in the ultraprecise $H_2{}^{16}O$ network relate to zero-pressure values, either through (*i*) measurements at very low (0.01 – 0.02 Pa) pressures, (*ii*) explicit extrapolation to zero pressure, or (*iii*) including the possible pressure-shift effects in the uncertainty budget. Hence, the listed values for the protected radio lines also pertain to zero-pressure values, with special relevance for the extremely low pressures in interstellar space.

5. CONCLUSION

In the present study, an ultraprecise spectroscopic network, corresponding to quantum states and transitions of the $H_2{}^{16}O$ water isotopologue has been extended and refined by the precise frequency calibration of 55 rovibrational transitions determined using the NICE-OHMS measurement technology. Of the 60 radio lines protected by the International Astronomical Union and the Panel on Frequency Allocations of the US National Academy of Sciences, 51 have been considerably improved in accuracy due to our present and previous Lamb-dip positions. Specifically, their uncertainties, falling into the 10 – 200 kHz range, have been brought to below 7.5 kHz. For the nine lowest-frequency transitions, all known with an accuracy better than 1 kHz, no improvements could be achieved. These lines play an essential role within the network, because they connect the *even*- and *odd*-parity levels of the ground vibrational state.

In principle, a similar analysis might be conducted for $H_2{}^{18}O$, as well. A large database of Lamb-dip lines has already been collected (Diouf et al. 2021), and a partial procedure for extracting radio lines from this database has been executed previously (Ubachs et al. 2024). For the HDO isotopologue, such a procedure was halted in view of parity-pair-mixing effects that limited the accuracy of the Lamb dips measured in Diouf et al. (2022a).

SUPPLEMENTAL INFORMATION

Additional data related to this work are available at https://zenodo.org/records/16757281. Table S1 contains a list of new experimental $H_2{}^{16}O$ rovibrational transitions recorded for the present paper with the NICE-OHMS technique at Amsterdam and Louvain-la-Neuve. Table S2 provides the paths within the ultraprecise $H_2{}^{16}O$ network for all radio lines given in Table II, the best paths defining radio frequencies, as well as the collection of data sources used in the comparison. Table S3 includes basic cycles associated with the shortest-path-based forest of the ultraprecise $H_2{}^{16}O$ spectroscopic network.

ACKNOWLEDGEMENTS

This work was funded by LASERLAB-EUROPE (grant no. 654148), a European Union's Horizon 2020 research and innovation programme. The present study is part of a European Partnership on a Metrology project, which is co-financed by the European Unionâ€™s Horizon Europe Research and Innovation Programme and by the Participating States (funder ID: 10.13039/100019599, grant no.: 23FUN04 COMOMET). The research performed in Budapest received support from the National Research, Development and Innovation Office of Hungary (NKFIH, grants K138233 and PD145972). A.A., A. B. and C. L. acknowledge the FNRS CDR (grant no. J.0113.23) and MIS (grant no. F.4038.24) for financial support.

REFERENCES

Bauer, A., Godon, M., Carlier, J., & Gamache, R. 1998, J. Quant. Spectrosc. Rad. Transf., 59, 273

Bauer, A., Godon, M., Kheddar, M., & Hartmann, J. 1989, J. Quant. Spectrosc. Rad. Transf., 41, 49

Brown, L. R., & Plymate, C. 1996, J. Quant. Spectrosc. Rad. Transf., 56, 263

Burenin, A. V., Fevralskikh, T. M., Karyakin, E. N., Polyansky, O. L., & Shapin, S. M. 1983, J. Mol. Spectrosc., 100, 182

Cazzoli, G., Puzzarini, C., Harding, M. E., & Gauss, J. 2009, Chem. Phys. Lett., 473, 21

Cazzoli, G., Puzzarini, C., & Lapinov, A. 2004, Astrophys J., 611, 615

Cernicharo, J., Goicoechea, J. R., Daniel, F., et al. 2006, Astrophys. J, 649, L33

Chance, K. V., Park, K., & Evenson, K. M. 1998, J. Quant. Spectrosc. Rad. Transf., 59, 687

Chen, J., Hua, T.-P., Tao, L.-G., et al. 2018, J. Quant. Spectrosc. Rad. Transf., 205, 91

Cheung, A. C., Rank, D. M., Townes, C. H., Thornton, D. D., & Welch, W. J. 1969, Nature, 221, 626â€“628

Committee on Radio Frequencies Board on Physics and Astronomy, National Academies of Sciences – Engineering – Medicine. 2015, Handbook of Frequency Allocations and Spectrum Protection for Scientific Uses (National Academy of Sciences, Washington, USA)

Coudert, L. H., Martin-Drumel, M.-A., & Pirali, O. 2014, J. Mol. Spectrosc., 303, 36

Coudert, L. H., Pirali, O., Vervloet, M., Lanquetin, R., & Camy-Peyret, C. 2004, J. Mol. Spectrosc., 228, 471

Cozijn, F. M. J., Dupré, P., Salumbides, E. J., Eikema, K. S. E., & Ubachs, W. 2018, Phys. Rev. Lett., 120, 153002

Császár, A. G., & Furtenbacher, T. 2011, J. Mol. Spectrosc., 266, 99

de Lucia, F. C., Helminger, P., Cook, R. L., & Gordy, W. 1972, Phys. Rev. A, 5, 487

Diouf, M. L., Tóbiás, R., Cozijn, F. M. J., et al. 2022a, Opt. Express, 30, 46040

Diouf, M. L., Tóbiás, R., Simkó, I., et al. 2021, J. Phys. Chem. Ref. Data, 50, 023106

Diouf, M. L., Tóbiás, R., van der Schaaf, T. S., et al. 2022b, Mol. Phys., 120, e2050430

Drouin, B. J., Yu, S., Pearson, J. C., & Gupta, H. 2011, J. Mol. Struct., 1066, 2

Endres, C. P., Schlemmer, S., Schilke, P., Stutzki, J., & MÄŁller, H. S. P. 2016, J. Mol. Spectrosc., 327, 95

Flaud, J.-M., Camy-Peyret, C., & Valentin, A. 1972, J. Phys. (Paris), 33, 741

Fleming, J. W., & Gibson, M. J. 1976, J. Mol. Spectrosc., 62, 326

Furtenbacher, T., Tóbiás, R., Tennyson, J., Polyansky, O. L., & Császár, A. G. 2020a, J. Phys. Chem. Ref. Data, 49, 033101

Furtenbacher, T., Tóbiás, R., Tennyson, J., et al. 2020b, J. Phys. Chem. Ref. Data, 49, 043103

Gianfrani, L., Hu, S.-M., & Ubachs, W. 2024, La Rivista del Nuovo Cimento, 47, 229â€“298

Golden, S., Wentink, T., Hillger, R., & Strandberg, M. W. P. 1948, Phys. Rev., 73, 92

Golubiatnikov, G. Y. 2005, J. Mol. Spectrosc., 230, 196

Golubiatnikov, G. Y., Markov, V. N., Guarnieri, A., & Knochel, R. 2006, J. Mol. Spectrosc., 240, 251

Guelachvili, G., & Rao, K. N. 1986, Handbook of Infrared Standards (Academic Press, Orlando)

Helminger, P., Messer, J. K., & de Lucia, F. C. 1983, Appl. Phys. Lett., 42, 309

Huiszoon, C. 1971, Rev. Sci. Instrum., 42, 477

Jen, C. K. 1951, Phys. Rev., 81, 197

Johns, J. W. C. 1985, J. Opt. Soc. Am. B, 2, 1340

Karlovets, E. V., Mikhailenko, S. N., Koroleva, A. O., & Campargue, A. 2024, J. Quant. Spectrosc. Rad. Transf., 314, 108829

Kassi, S., Lauzin, C., Chaillot, J., & Campargue, A. 2022, Phys. Chem. Chem. Phys., 24, 23164

Kassi, S., Stoltmann, T., Casado, M., Daeron, M., & Campargue, A. 2018, J. Chem. Phys., 148, 054201

Kauppinen, J., Kärkkäinen, T., & Kyrö, E. 1978, J. Mol. Spectrosc., 71, 15

Kauppinen, J., & Kyrö, E. 1980, J. Mol. Spectrosc., 84, 405

King, W. C., & Gordy, W. 1954, Phys. Rev., 93, 407

Koshelev, M. A. 2011, J. Quant. Spectrosc. Rad. Transf., 112, 550

Koshelev, M. A., Tretyakov, M. Y., Golubiatnikov, G. Y., et al. 2007, J. Mol. Spectrosc., 241, 101

Kukolich, S. G. 1969, J. Chem. Phys., 50, 3751

Markov, V. N., & Krupnov, A. F. 1995, J. Mol. Spectrosc., 172, 211

Matsushima, F., Odashima, H., Iwasaki, T., Tsunekawa, S., & Takagi, K. 1995, J. Mol. Spectrosc., 352, 371

Messer, J. K., de Lucia, F. C., & Helminger, P. 1983, Int. J Infrared Milli., 4, 505

Miani, A., & Tennyson, J. 2004, J. Chem. Phys., 120, 2732

Mikhailenko, S. N., Béguier, S., Odintsova, T. A., et al. 2020, J. Quant. Spectrosc. Rad. Transf., 253, 107105

Mikhailenko, S. N., Karlovets, E. V., Koroleva, A. O., & Campargue, A. 2024, J. Phys. Chem. Ref. Data, 53

Mikhailenko, S. N., Mondelain, D., Karlovets, E. V., Kassi, S., & Campargue, A. 2018, J. Quant. Spectrosc. Rad. Transf., 206, 163

Müller, H. S. P., Schlöder, F., Stutzki, J., & Winnewisser, G. 2005, J. Mol. Struct., 742, 215

NIST/SEMATECH. 2012, NIST/SEMATECH e-Handbook of Statistical Methods, Measurement Process Characterization, Section 2.5.7, https://www.itl.nist.gov/div898/handbook/mpc/section5/mpc57.htm

Partridge, R. H. 1981, J. Mol. Spectrosc., 87, 429

Pickett, H., Poynter, R., Cohen, E., et al. 1998, J. Quant. Spectrosc. Rad. Transf., 60, 883

Ritz, W. 1908, Astrophys. J., 28, 237

Solomon, P., & Klemperer, W. 1972, Astrophys. J., 178, 389

Steenbeckeliers, G., & Bellet, J. 1971, C. R. Acad. Sci. B Phys., 273, 471

Stephenson, D. A., & Strauch, R. G. 1970, J. Mol. Spectrosc., 35, 494

Supplee, J. M., Whittaker, E. A., & Lenth, W. 1994, Appl. Opt., 33, 6294

Tielens, A., & Hagen, W. 1982, Astron. Astrophys., 114, 245

Tóbiás, R., Diouf, M. L., Cozijn, F. M., Ubachs, W., & Császár, A. G. 2024, Commun. Chem., 7, 34

Tóbiás, R., Furtenbacher, T., Simkó, I., et al. 2020, Nat. Commun., 11, 1708

Toureille, M., Koroleva, A. O., Mikhailenko, S. N., Pirali, O., & Campargue, A. 2022, J. Quant. Spectrosc. Rad. Transf., 291, 108326

Townes, C. H., & Merritt, F. R. 1946, Phys. Rev., 70, 558

Tretyakov, M. Y., Koshelev, M. A., Vilkov, I. N., Parshin, V. V., & Serov, E. A. 2013, J. Quant. Spectrosc. Rad. Transf., 114, 109

Ubachs, W., Császár, A. G., Diouf, M. L., Cozijn, F. M., & Tóbiás, R. 2024, ACS Earth Space Chem., 8, 1901

van Dishoeck, E. F., Herbst, E., & Neufeld, D. A. 2013, Chem. Rev., 113, 9043

WeiĂź, A., De Breuck, C., Marrone, D. P., et al. 2013, Astrophys. J., 767, 88

Wright, C. M., van Dishoeck, E. F., Black, J. H., et al. 2000, Astron. Astrophys., 358, 89

Yu, S., Pearson, J. C., & Drouin, B. J. 2013, J. Mol. Spectrosc., 288, 7

Yu, S., Pearson, J. C., Drouin, B. J., et al. 2012, J. Mol. Spectrosc., 279, 16